Delft University of Technology

Modeling of Liquid Injectivity in Surfactant-Alternating-Gas Foam Enhanced Oil Recovery

Gong, Jiakun; Vincent-Bonnieu, Sebastien; Kamarul Bahrim, Ridhwan Zhafri; Che Mamat, Che Abdul Nasser Bakri; Tewari, Raj Deo; Groenenboom, Jeroen; Farajzadeh, Rouhi; Rossen, Bill

Important note
To cite this publication, please use the final published version (if applicable).
Please check the document version above.

Modeling of Liquid Injectivity in Surfactant-Alternating-Gas Foam Enhanced Oil Recovery

J. Gong, Delft University of Technology; **S. Vincent-Bonnieu,** Shell Global Solutions International B.V.;
R. Z. Kamarul Bahrim, C. A. N. B. Che Mamat, and **R. D. Tewari,** Petronas;
J. Groenenboom, Shell Global Solutions International B.V.; **R. Farajzadeh,** Delft University of Technology
and Shell Global Solutions International B.V.; and **W. R. Rossen,** Delft University of Technology

Summary

Surfactant alternating gas (SAG) is often the injection strategy used for injecting foam into a reservoir. However, liquid injectivity can be very poor in SAG, and fracturing of the well can occur. Coreflood studies of liquid injectivity directly following foam injection have been reported. We conducted a series of coreflood experiments to study liquid injectivity under conditions more like those near an injection well in a SAG process in the field (i.e., after a period of gas injection). Our previous experimental results suggest that the injectivity in a SAG process is determined by propagation of several banks. However, there is no consistent approach to modeling liquid injectivity in a SAG process. The Peaceman equation is used in most conventional foam simulators for estimating the wellbore pressure and injectivity.

In this paper, we propose a modeling approach for gas and liquid injectivity in a SAG process on the basis of our experimental findings. The model represents the propagation of various banks during gas and liquid injection. We first compare the model predictions for linear flow with the coreflood results and obtain good agreement. We then propose a radial-flow model for scaling up the core-scale behavior to the field. The comparison between the results of the radial-propagation model and the Peaceman equation shows that a conventional simulator based on the Peaceman equation greatly underestimates both gas and liquid injectivities in a SAG process. The conventional simulator cannot represent the effect of gas injection on the subsequent liquid injectivity, especially the propagation of a relatively small region of collapsed foam near an injection well. The conventional simulator's results can be brought closer to the radial-flow-model predictions by applying a constant negative skin factor.

The work flow described in this study can be applied to future field applications. The model we propose is based on a number of simplifying assumptions. In addition, the model would need to be fitted to coreflood data for the particular surfactant formulation, porous medium, and field conditions of a particular application. The adjustment of the simulator to better fit the radial-flow model also would depend, in part, on the grid resolution of the near-well region in the simulation.

Introduction

In gas-injection enhanced oil recovery (EOR), gas can be injected either alone or in combination with water injection, usually in a water-alternating-gas process. However, gas-injection EOR often suffers from poor sweep efficiency, which can make the process uneconomical. The gas sweep efficiency can be reduced by gravity override and gas breakthrough in high-permeability zones. Both problems are made worse by the low viscosity of gas (Lake et al. 2014). Foam can improve the sweep efficiency in gas-injection EOR (Schramm 1994; Rossen 1996).

Foam is injected into reservoirs mainly in two ways: coinjecting gas and surfactant solution and alternatively injecting gas slugs and surfactant-solution slugs (Matthews 1989; Heller 1994; Schramm 1994; Rossen 1996; Kibodeaux and Rossen 1997; Shan and Rossen 2004; Rossen et al. 2010). This second approach, known as SAG, is the most common method of injection for foam EOR, for operational reasons and for its excellent injectivity during gas injection. Injectivity is the key economical factor of a foam EOR process. However, liquid injectivity is usually very poor in SAG, and fracturing of an injection well can occur (Kuehne et al. 1990; Martinsen and Vassenden 1999).

Most of the literature on liquid injectivity following foam is related to foam diversion in matrix acid well-stimulation treatments (Kibodeaux et al. 1994; Zeilinger et al. 1995; Nguyen et al. 2003; Nguyen et al. 2009b). The goal in an acid-stimulation process is to reduce injectivity to the greatest possible extent. However, very poor liquid injectivity in a SAG process slows injection of the liquid slug and harms process economics. Therefore, excessively poor liquid injectivity should be avoided.

The liquid injectivity in a foam-acid diversion process was previously studied in coreflood experiments. Kibodeaux et al. (1994) found that water relative permeability (k_{rw}) rose immediately by a factor of approximately 5 during liquid injection directly following foam. Liquid mobility was constant for a time, and then rose again by a large factor, in a slow-moving wave from the inlet to the outlet of the core. Gas dissolution into unsaturated liquid within the fingers would account for the rise in liquid saturation within the fingers.

Computed-tomography (CT) experiments of liquid injection following foam (Nguyen et al. 2009a, 2009b) confirmed that liquid displaced gas in one or two fingers through the core, leaving the rest of the foam in place. Unlike conventional fingering, in which the front is increasingly nonuniform as it advances, eventually forming fingers, liquid displaces foam only in these fingers right from the inlet of the core. This suggested that it was not simply viscous fingering but trapping of gas in place by the foam. CT images also confirmed that with time, liquid saturation rises within the fingers, suggesting that gas trapped within the fingers dissolved into surrounding unsaturated liquid.

In a separate paper (Gong et al. 2019), we report coreflood experiments on liquid injectivity under conditions such as those near an injection well in a SAG application in the field (i.e., after a prolonged period of gas injection following nitrogen foam). We found that conditions very near the well, crucial to injectivity, are substantially different from those farther out, and are not described by the

current foam models. The results can guide development of a simple model for liquid injectivity on the basis of radial propagation of the various banks seen in the experiments.

Liquid injectivity directly following foam is very poor, as shown in previous studies (Kibodeaux et al. 1994; Zeilinger et al. 1995). Liquid first fingers through foam, and then it dissolves gas trapped within the fingers, and the overall mobility rises sharply. During prolonged gas injection after foam, however, a region forms near the inlet and slowly propagates downstream. In this region, the gas mobility is much greater. The abrupt rise in the gas mobility appears to reflect the decline in water saturation below approximately 0.2 in our experiments (Zhou and Rossen 1995; Khatib et al. 1998). This decline in water saturation in the corefloods reflects, in part, liquid evaporation and also pressure-driven flow and capillary effects on the core scale. Foam completely collapses or greatly weakens within this region. In this region of lower liquid saturation, the liquid mobility during subsequent liquid injection is much greater than downstream, and the liquid sweeps the entire core cross section rather than one or more fingers. The mobility in the region of liquid fingering is insensitive to the quality of foam injected before gas and during the period of gas injection (though the size of the region grows with longer gas injection). These results suggest that in the field, there is a small region very near the well that is crucial to the overall injectivity in which the liquid mobility is much greater than that farther from the well.

Leeftink et al. (2015) have shown the difficulties in accurately simulating the gas injectivity in SAG. The gas injectivity is dominated by the near-well saturation and mobilities, which are not represented well in conventional simulators. Conventional simulators also fail to represent the shock past the region of lowest mobility during gas injection in SAG (Rossen 2013). Modeling of the liquid injectivity in SAG remains largely unexplored.

In this paper, we fit a model to our coreflood experiments. The model is based directly on the laboratory data, although it involves many assumptions and approximations. Nevertheless, at this time, it is the most direct way to represent our laboratory findings in a model for field application.

We first propose a linear-flow model for both the gas-injection period and the following liquid-injection period in a SAG process. The model reflects the propagation of various banks. The dimensionless propagation velocities and mobilities of various banks that serve as inputs of the linear-flow model are derived from the coreflood experiments. The positions of the front of the various banks are determined by the dimensionless propagation velocities, which are determined in the experiments in terms of local pore volume (LPV) [i.e., the volume injected divided by the cumulative pore volume (PV) from a given position back to the inlet]. The dimensionless velocity is thus defined as (PV in place)/(PV injected) as the front advances. For example, according to the experimental results, during gas injection, the collapsed-foam bank reaches the end of each section after approximately 400 LPV of gas injection. In other words, the collapsed-foam bank propagates with a dimensionless velocity $V = 1/400$. The total mobilities ($\nabla p/u_t$) of various banks are determined from the pressure gradient (∇p) and total superficial velocity (u_t) by applying Darcy's law. We compare the experimental results and the model predictions described later in the text and show a good fit.

We then apply this model to an injection well in a field application. We assume that the core-scale behavior can be scaled up directly to the field, and that the various banks propagate from the injection well radially. The same dimensionless propagation velocities and mobilities of the various banks obtained from the coreflood experiments are applied to the radial-flow model. We compare our results to the injectivity estimated using the Peaceman equation (Peaceman 1978) in a gridblock as in a conventional foam simulator. We point out the potential errors when a conventional simulator computes the injectivity of gas and liquid in a SAG process. We also explore the possibility of reconciling the results of the radial-flow model and the Peaceman equation by applying a constant negative skin factor.

Brief Summary of Experimental Results

The coreflood experiments were conducted in a setup schematically shown in **Fig. 1.** In our coreflood experiments, we injected nitrogen foam, gas (nitrogen), and surfactant solution, with an alpha olefin sulfonate concentration of 0.5 wt% and 3 wt% salinity, into a 17-cm-long Berea core at 90°C with 40-bar backpressure to minimize the gas-expansion effects. Steady-state foam is generated first, and then surfactant solution is injected directly following foam injection, or following prolonged periods of gas injection following foam. Pressure differences are measured separately across five sections of the core and supplemented with CT scans to relate water saturation to mobilities. (The third sectional pressure difference is the difference between absolute-pressure measurements P_2 and P_3.) To avoid entrance-region and capillary-end effects, we used only the data of the three middle sections, without considering the sections near the inlet and outlet. We examined liquid injectivity in two situations: liquid injection directly following foam injection, as in previous studies, and liquid injection following prolonged periods of gas injection following foam, to reflect the injectivity near the injection well in a SAG process. Our experimental results suggest that the injectivity in a SAG process is determined by the propagation of various banks, as illustrated in **Figs. 2 and 3.**

Briefly, if liquid injection follows foam directly, liquid first enters the core with low relative permeability, then fingers through the foam; thereafter, trapped gas within the liquid fingers dissolves into unsaturated liquid. This is confirmed by pressure-gradient measurements and CT images. If gas injection follows foam, a bank of collapsed or greatly weakened foam propagates slowly from the inlet. During subsequent liquid injection, liquid quickly saturates the collapsed-foam bank and then penetrates the weakened-foam bank ahead of the collapsed-foam bank in a way similar to liquid injection directly after foam. Subsequently, a second bank develops within the liquid-fingering bank, in which gas has dissolved within the fingers, and the mobility rises substantially. These are also confirmed by pressure-gradient measurements and CT images. Therefore, there are five banks whose velocities and total mobilities must be specified: during gas injection, the foam bank and the collapsed-foam bank; during liquid injection, the bank of liquid saturating the collapsed-foam region; and thereafter, the banks of liquid fingering through foam and of gas dissolving within the fingers in that bank.

The dimensionless propagation velocities and mobilities of the various banks derived from experimental results are listed in **Table 1.** These are the inputs for the linear-flow and radial-flow models used in this study. In the plots below, coreflood results are presented in terms of total pore volumes (TPVs) (i.e., volumes injected divided by the TPV of the core).

Linear-Flow Model

Model Description. In the linear-flow model, we consider a 17-cm-long cylindrical core, as in the coreflood experiments. The region of interest is assumed to be homogeneous. The permeability is 150 md, which is the average value of the permeabilities of different sections of the core used in our experiments. The porosity is 0.2.

As discussed previously, the region of interest is considered to be occupied by various banks. The total mobilities of the various banks are assumed to be uniform in each bank. The dimensionless propagation velocities and total mobilities of the various banks are estimated from the experiments, as listed in Table 1.
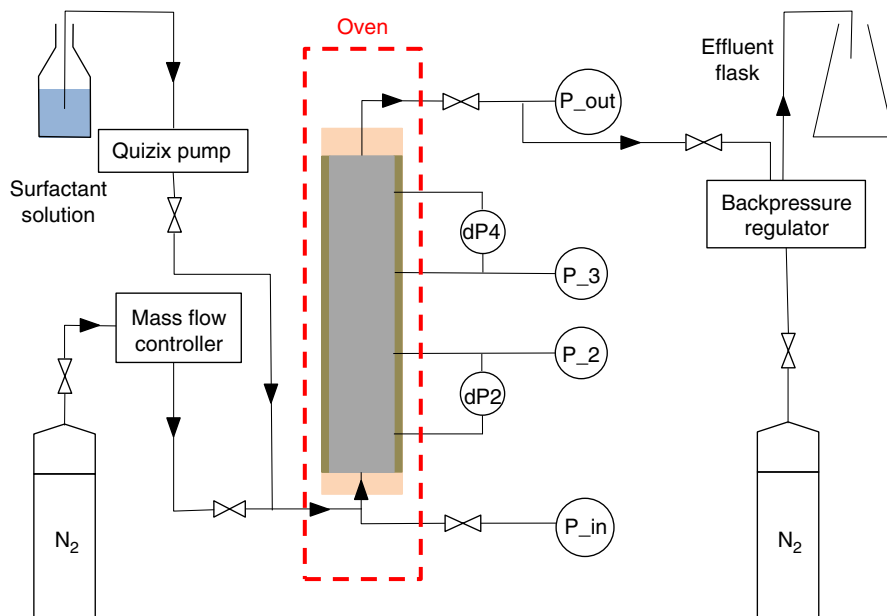
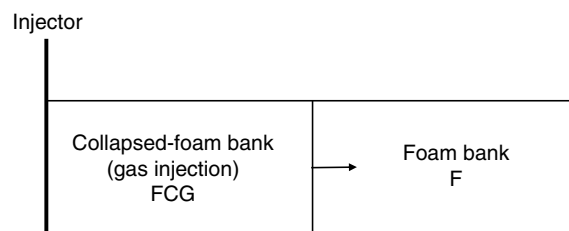**Fig. 1—A schematic of the coreflood experimental setup.**

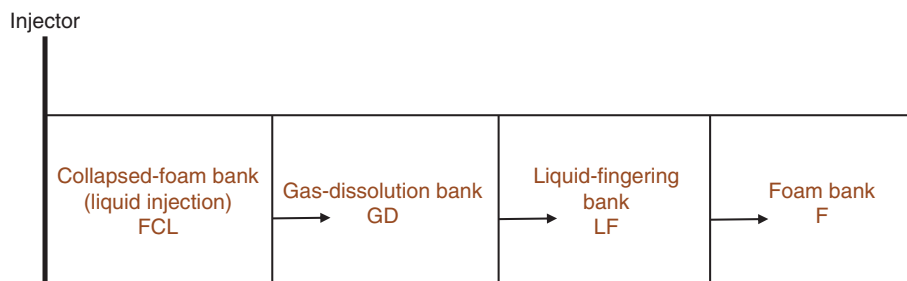**Fig. 2—Banks during gas-injection period in a SAG process.**

Fig. 3—Banks during liquid-injection period in a SAG process.

Period	Bank	Dimensionless Velocity	Total Mobility (m²/Pa·s)
Gas injection	Collapsed-foam bank	2.5×10^{-3}	8.97×10^{-10}
Gas injection	Foam bank	Initially present*	1.25×10^{-11}
Gas injection	Water	Initially present*	1.50×10^{-10}
Liquid injection	Liquid slug in collapsed-foam region	0.78	1.47×10^{-10}
Liquid injection	Liquid-fingering bank	3.33	8.50×10^{-13}
Liquid injection	Gas-dissolution bank	0.08	6.63×10^{-11}
Liquid injection	Foam bank	Initially present	1.25×10^{-11}

*In the corefloods, the initial state of the core is foam. In the radial-flow model, we assume that initially the formation is saturated with liquid, $S_w = 1$. Foam advances in this case with a dimensionless velocity of unity.

Table 1—Dimensionless propagation velocities and mobilities of the various banks in a SAG process.

For the gas-injection period in a SAG process, we assume foam fills the core at the start, and the foam bank has a uniform mobility ahead of a collapsed-foam bank. More-sophisticated models of mobility during relatively early periods of gas injection (the first few PVs) are described by Shan and Rossen (2004), Rossen and Boeije (2015), and Leeftink et al. (2015). Our main interest here lies in the effect of previous gas injection on subsequent liquid injectivity. The total pressure difference during gas injection is the sum of the pressure differences across the foam bank Δp_F and the collapsed-foam bank Δp_{FCG} (as long as each bank is represented in the core):

$$\Delta p_t = \Delta p_F + \Delta p_{FCG}. \quad \dots \dots \dots \dots \dots \dots \dots \dots \dots \dots \dots \dots \dots \dots \dots \dots \dots \dots \dots \dots \dots \dots (1)$$

For the liquid-injection period, the total pressure difference is the sum of the pressure differences across the collapsed-foam bank (Δp_{FCL}), the gas-dissolution bank (Δp_{GD}), the liquid-fingering bank (Δp_{LF}), and the foam bank (Δp_F) (as long as each bank is represented in the core),

$$\Delta p_t = \Delta p_{FCL} + \Delta p_{GD} + \Delta p_{LF} + \Delta p_F. \quad \dots \dots \dots \dots \dots \dots \dots \dots \dots \dots \dots \dots \dots \dots \dots \dots \dots \dots \dots (2)$$

For each bank, Darcy's law for linear multiphase flow is used to calculate the pressure difference,

$$\Delta p_b = \int_{l_1}^{l_2} \frac{Q_t}{A\lambda_t(b)}\,dl = \frac{Q_t}{A}\frac{(l_2 - l_1)}{\lambda_t(b)}, \quad \dots \dots \dots \dots \dots \dots \dots \dots \dots \dots \dots \dots \dots \dots \dots \dots \dots (3)$$

where, in each bank, extending from positions l_1 to l_2, the total mobility [$\lambda_t(b)$] is assumed to be uniform.

For comparison with the sectional pressure differences measured in the linear corefloods, a similar calculation is carried out below for each section, based on the banks present in that section.

Results for Linear Flow. Fig. 4 shows the comparison results of the linear-flow model and the coreflood experiment. Initially, the pressure gradient in the experiment is much larger than that in the model. For simplicity, we do not attempt to represent the period of initial gas injection. More importantly, the initial state of the core in the experiment (strong, steady-state foam injected at fixed quality) is not that in the field (gas injection following a liquid slug) [see Shan and Rossen (2004) and Leeftink et al. (2015)]. Therefore, mobility at the start of the injection of the gas slug (following foam) is not representative of gas injection in the field (following injection of a liquid slug).
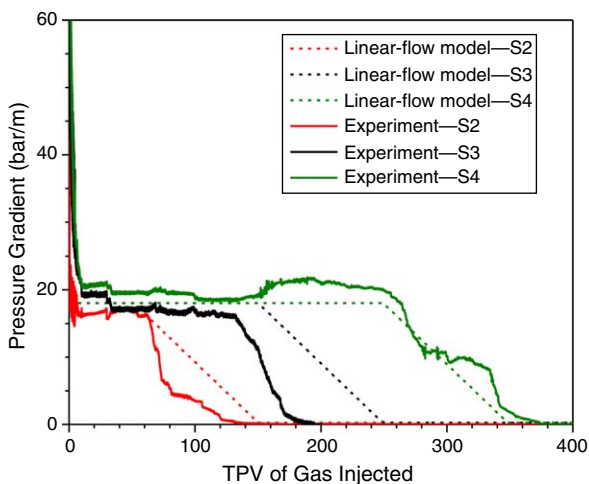

Fig. 4—Comparison of the pressure gradient in the coreflood experiment and the linear-flow model during the gas-injection period.

After this initial period, mobility is nearly constant until a large volume of gas is injected (the plateau in pressure gradient in Fig. 4). After approximately 400 LPV of gas injection, the total mobility increases greatly, reflecting foam collapse or great weakening (the decline in the pressure gradient in the figure). The front of the collapsed-foam bank advances with a dimensionless velocity of 1/400. In general, the linear-flow model gives a reasonable fit to the laboratory data. In Sections 2 (S2) and 3 (S3), foam collapse takes a somewhat shorter time in the experiment than in the linear-flow model. One of the possible reasons is that we assume the same dimensionless propagation velocity of the collapsed-foam bank for all three sections. However, in reality, drying out and collapse of foam reflects the interplay of pressure gradient, capillary effects, and evaporation. This could lead to different dimensionless velocities for different sections along the core. In the absence of data at longer distances, we choose the velocity based on Section 4 (S4) as the best value for scaling to longer distances.

For the liquid-injection period, the pressure gradient is strongly affected by the size of the gas slug previously injected **(Figs. 5 and 6)**. The collapsed-foam bank penetrates S2 after 135-TPV gas injection (Fig. 5). It fills S2 and S3 and penetrates a bit into S4 after 245-TPV gas injection (Fig. 6). The pressure gradient of S3 during liquid injection following 135-TPV gas injection is approximately 45 bar/m (Fig. 5), but is only approximately 5 bar/m in the experiment in which 245 TPV of gas was injected (Fig. 6). The pressure gradient during liquid injection is much lower if foam collapses or strongly weakens in the corresponding section (or in a large part of it).

As shown in Fig. 5, the plateau values of the pressure gradient for S3 and S4 are the same in the linear-flow model, because we assume the same permeability and total mobility for the two sections. However, the pressure gradients for S3 and S4 are different in the

experiment. The main reason is that the permeabilities of S3 and S4 are different: 184 md for S3 and 134 md for S4, respectively. The permeability ratio of approximately 1.35 explains most of the discrepancy in the plateau pressure gradients of the two sections in the experiment.
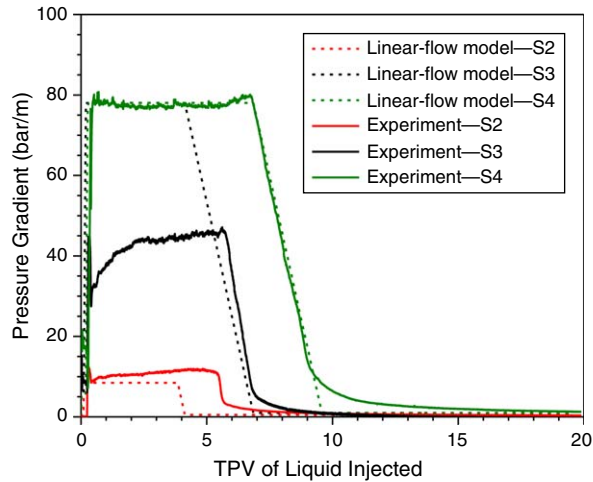

Fig. 5—Comparison of the pressure gradient in the coreflood experiment and the linear-flow model during the liquid-injection period following 135-TPV gas injection.
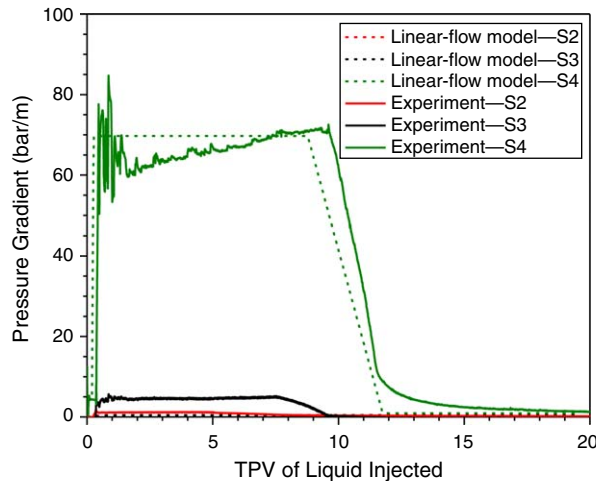

Fig. 6—Comparison of the pressure gradient in the coreflood experiments and the linear-flow model during the liquid-injection period following 245-TPV gas injection. The model fits for S2 and S3 overlay the horizontal axis.

Radial-Flow Model

Model Description. The radial-flow model is based on the findings from our coreflood experiments. We assume the core-scale behavior could be scaled up directly to field, and that the various banks (Table 1) propagate with the same dimensionless velocity in radial flow as was used to fit the coreflood experiments.

The wellbore radius (r_w) here is 0.1 m. The outer radius (r_e) is 20 m, which corresponds to the equivalent radius (r_e) of a 100×100-m block containing the well (Peaceman 1978). The porosity (ϕ) is 0.2, and the permeability is 150 md, as in the linear-flow model.

The total mobilities and dimensionless propagation velocities of the various banks are the same as in the linear-flow model (Table 1), derived from our coreflood experiments. We express the dimensionless time and gas- and liquid-slug sizes in terms of the PV of a 100×100-m gridblock, which corresponds to the conventional-simulator solution below. We assume the region around the well is initially fully saturated with water, which is displaced by foam with a dimensionless velocity of unity.

For the gas-injection period, the total pressure difference is the sum of pressure differences in the foam bank, the collapsed-foam bank, and, for a time, the water bank ahead of foam. For the liquid-injection period, the total pressure difference is the sum of pressure differences in the collapsed-foam bank, the gas-dissolution bank, the liquid-fingering bank, and the foam bank. After an amount of gas or liquid injection (at each timestep), the dimensionless propagation velocities are used to determine the positions of the front of the various banks. For each bank, Darcy's law for radial multiphase flow is used to calculate the pressure difference:

$$\Delta p_b = \int_{r_1}^{r_2} \frac{Q_t}{2\pi r h \lambda_t(b)} dr = \frac{Q_t}{2\pi h} \frac{1}{\lambda_t(b)} \ln\left(\frac{r_2}{r_1}\right), \quad \text{.............................} \quad (4)$$

where in each bank, extending from r_1 to r_2, the total mobility [$\lambda_t(b)$] is assumed to be uniform.

For the radial-flow model, we compared the pressure difference between r_w and r_e to the pressure difference caused by injecting water at the same volumetric rate into a fully water-saturated region. The dimensionless pressure difference (P_D) is then defined as

$$P_D = \frac{\Delta p_t}{(\Delta p_t)_{S_w=1}} = \frac{\Delta p_t}{\dfrac{Q_t}{2\pi h \lambda_w} \ln\left(\dfrac{r_2}{r_1}\right)}, \quad \dots\dots\dots\dots\dots\dots\dots\dots\dots\dots\dots\dots\dots\dots\dots\dots\dots\dots\dots\dots \quad (5)$$

where λ_w is the water mobility of a fully water-saturated region ($S_w = 1$).

Results for Radial-Flow Model. Fig. 7 shows the dimensionless pressure drop as a function of volume of gas injected. During gas injection, the collapsed-foam bank propagates from the injection well. Similar behavior is shown for different volumes of gas injection.
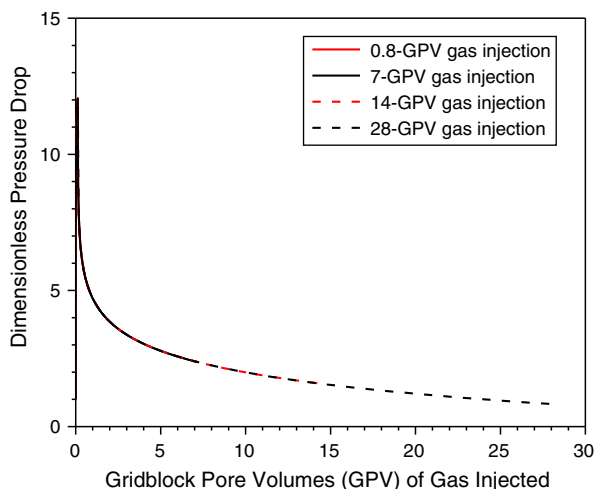

Fig. 7—Dimensionless pressure drop surrounding the injection well during the gas-injection period in a SAG process. The solid and dashed lines overlie each other in this plot.

Similar to the sectional pressure differences in the corefloods, to illustrate the advance of the various banks around the well, we also present dimensionless pressure differences between r_w and $(1/4)r_e$, between $(1/4)r_e$ and $(1/2)r_e$, between $(1/2)r_e$ and $(3/4)r_e$, and between $(3/4)r_e$ and r_e. **Fig. 8** shows these sectional pressure differences. The pressure difference decreases greatly as foam collapses or strongly weakens in the corresponding region. The first region, from r_w to $(1/4)r_e$, plays a larger role in the total pressure rise at the well.
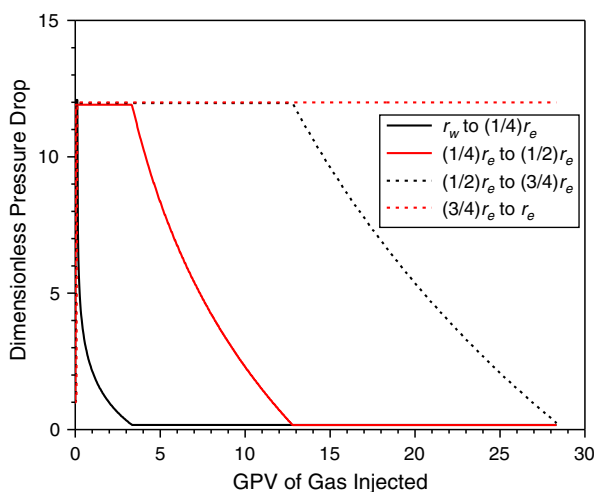

Fig. 8—Dimensionless pressure drop as a function of distance from the injection well during gas injection: effect of the propagation of the collapsed-foam region.

Fig. 9 shows the dimensionless pressure drop between r_w and r_e during liquid injection under different conditions: liquid injection directly following foam or following various periods of gas injection. When liquid is injected directly following foam, the liquid injectivity is approximately 65 times worse than injecting liquid into a water-saturated region without foam. This is the worst case for liquid injectivity. A relatively small amount [e.g., 0.8 gridblock PV (GPV)] of gas injection does not help improve liquid injectivity much. As the volume of gas injected increases from 7 to 28 GPV, the dimensionless pressure drop during subsequent liquid injection decreases from approximately 35 to 10. This indicates that a larger gas slug creates a larger collapsed-foam region around the well, and, in turn, increases the subsequent liquid injectivity. The larger the gas-slug size, the better the subsequent liquid injectivity.
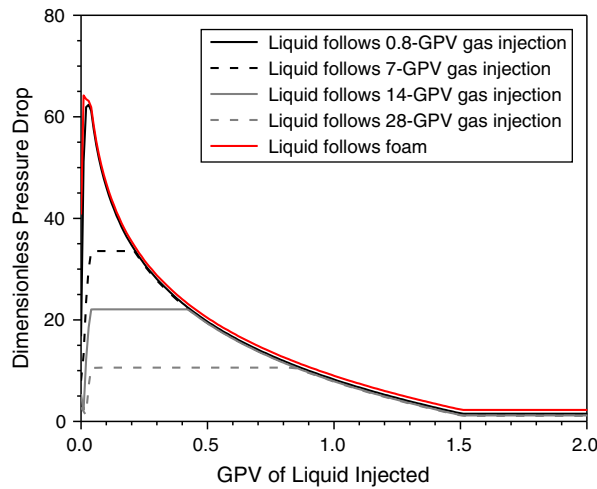
Fig. 9—Dimensionless pressure drop surrounding the injection well during the liquid-injection period in a SAG process. The curve for "liquid follows foam" is above the curve for "liquid follows 0.8-GPV gas injection" and nearly overlie each other at very short times.

Conventional Simulation Based on the Peaceman Equation. There are two types of approaches to simulate foam. Population-balance models (Kovscek and Radke 1994, Kam et al. 2007) attempt to represent the mechanisms of creation and destruction of liquid films, or lamellae, that separate gas bubbles, along with the effect of bubble size and other factors on the gas mobility. Implicit-texture (IT) models (Patzek and Myhill 1989; Cheng et al. 2000) represent the effect of foam on gas mobility by reducing the gas mobility through a mobility-reduction factor that depends on the water saturation, surfactant concentration, superficial velocities, and other factors. The IT models assume local equilibrium between the dynamics of creating and destroying bubbles. In this study, we use the widely used IT model in the STARS™ simulator (Cheng et al. 2000; CMG 2006). Details can be found in Appendix A.

The following assumptions are made for the calculations based on the Peaceman equation. Oil is not present in the region of interest, and water, gas, and rock are assumed to be incompressible. The reservoir is of a uniform height (h), and the vertical injection well penetrates the entire interval. We do not consider the effect of gravity, and foam immediately reaches local equilibrium. The water saturation in the gridblock is uniform at all times. Dispersion and viscous fingering are not considered, and the gridblock is assumed to be fully water saturated ($S_w = 1$) at the start of gas injection.

Our focus is the near-wellbore area, which is represented as a gridblock, as in reservoir simulators (CMG 2006; Schlumberger 2010). A wellbore of radius (r_w, 0.1 m) is located in a square gridblock of size $L \times L$, which is surrounded by four gridblocks. The gridblock size L is set at 100 m in this study (**Fig. 10**).
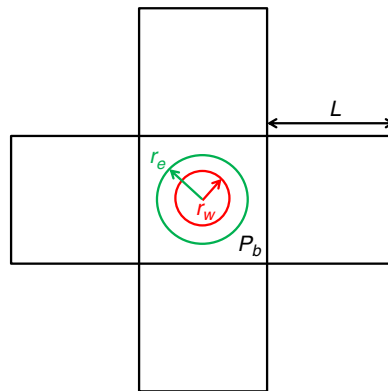

Fig. 10—Model for simulation. The wellbore radius r_w is greatly exaggerated here to make it visible.

We apply the algorithm of a conventional simulator to calculate the rise in well pressure during gas and liquid injection. Specifically, we determine the gridblock water saturation as a function of time using a material balance on the gridblock containing the injection well. The material balance on water can be described by Eqs. 6 and 7:

$$Q_i^{in} = Q_w^{out} + Q_g^{out}, \qquad\qquad\qquad\qquad\qquad\qquad\qquad\qquad\qquad\qquad\qquad\qquad\qquad (6)$$

$$L^2 h \phi \frac{dS_w}{dt} = Q_w^{in} - Q_w^{out}, \qquad\qquad\qquad\qquad\qquad\qquad\qquad\qquad\qquad\qquad\qquad (7)$$

where S_w is the water saturation in the gridblock, $i = w$ is for the liquid-injection period, and $i = g$ is for the gas-injection period.

For simplicity, we assume upwind weighting in the flux determination. The uniform water saturation of the central gridblock (S_w) can be calculated from

$$L^2 h \phi \frac{dS_w}{dt} = Q_w^{in}[f_w^{in} - f_w(S_w)], \qquad\qquad\qquad\qquad\qquad\qquad\qquad\qquad\qquad (8)$$

where $f_w^{in} = 0$ for gas injection, $f_w^{in} = 1$ for liquid injection, and

$$f_w = \left[1 + \frac{k_{rg}^f(S_w)}{\mu_g} \frac{\mu_w}{k_w(S_w)} \right]^{-1}, \quad \dots\dots\dots\dots\dots\dots\dots\dots\dots\dots\dots\dots\dots\dots\dots\dots \quad (9)$$

where μ_w and μ_g are the water and gas viscosities and $k_{rg}^f(S_w)$ is the foam-reduced gas relative permeability, which incorporates the effects of foam.

We then apply the Peaceman equation (1978) to calculate the pressure rise in the injection well. In most simulators, the Peaceman equation is used to describe the pressure difference between the injection well and the gridblock containing the injection well. Peaceman (1978) defined an equivalent radius (r_e) as the radius at which the steady-state flowing pressure in the reservoir is equal to the numerically calculated pressure of the gridblock (P_b) containing the well. The value of r_e is conventionally set to 0.2 L for a square gridblock (Peaceman 1978). The pressure difference between the injection well and the gridblock ΔP_t can be calculated as follows:

$$P_{r_e} = P_b, \quad \dots\dots\dots\dots\dots\dots\dots\dots\dots\dots\dots\dots\dots\dots\dots\dots\dots\dots\dots\dots\dots\dots \quad (10)$$

$$\Delta P_t = P_w - P_{r_e} = \frac{Q_i^{in}}{2\pi h k \lambda_{rt}} \ln \frac{r_e}{r_w}, \quad \dots\dots\dots\dots\dots\dots\dots\dots\dots\dots\dots\dots\dots\dots \quad (11)$$

where λ_{rt} is the total relative mobility and is defined as

$$\lambda_{rt} = \left[\frac{k_{rw}(S_w)}{\mu_w} + \frac{k_{rg}^f(S_w)}{\mu_g} \right]. \quad \dots\dots\dots\dots\dots\dots\dots\dots\dots\dots\dots\dots\dots\dots\dots \quad (12)$$

The effect of foam on gas relative permeability in the model is described in Appendix A. We fit foam-model parameters to data for foam apparent viscosity as a function of gas fractional flow (foam quality), as described in Appendix A, using the method of Boejie and Rossen (2015) and Farajzadeh et al. (2015).

Fig. 11 shows the dimensionless pressure drop during gas injection as a function of GPVs of gas injected. The peak value of the dimensionless pressure drop is approximately 1,100, which means the worst injectivity in gas injection is approximately 1,100 times lower than injecting water into a water-saturated region. Even at the later stage, the gas injectivity is 50 times lower than the reference injectivity.
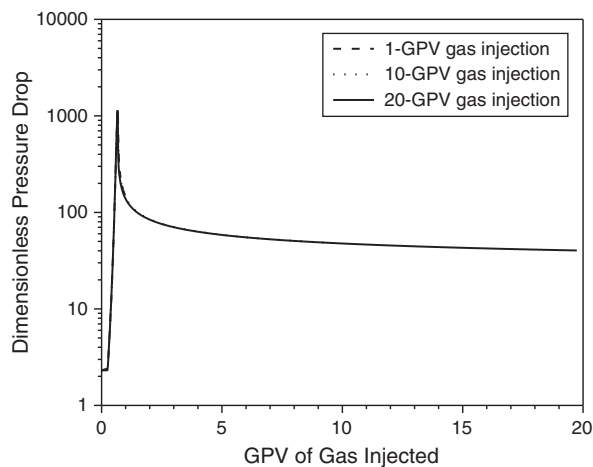

Fig. 11—Dimensionless pressure drop during gas injection, calculated with the Peaceman equation. The dotted, dashed, and solid lines overlie each other.

Fig. 12 shows water saturation in the gridblock containing the injection well. According to the simulation, S_w in the gridblock barely changes after approximately 1 GPV of gas injection.

Fig. 13 illustrates the dimensionless pressure drop during liquid injection following various periods of gas injection (i.e., 1, 10, and 20 GPV). The curves for liquid injection following different periods of gas injection are nearly identical because the liquid saturation in the gridblock at the start of liquid injection is nearly the same (Fig. 12). In the simulation model, the duration of the previous gas-injection period makes virtually no difference to subsequent liquid injectivity.

As shown in **Fig. 14,** S_w in the gridblock follows nearly the same trend during the liquid-injection period, no matter how much gas was previously injected. Liquid saturation in the gridblock is nearly constant after approximately 0.5 GPV of liquid injection.

Comparison of Injectivity Calculated With the Peaceman Equation and the Radial-Flow Model. In this subsection, we compare the injectivity calculated by the conventional model based on the Peaceman equation and by the radial-flow model, with respect to both gas and liquid injection in a SAG process.

As shown in **Fig. 15,** the simulation using the Peaceman equation underestimates gas injectivity by as much as 100 times for the minimum value and 50 times for the gas injectivity at a later stage. If the injection pressure is the limiting factor rather than the injection rate, as in this study, the injection rate would be as much as 100 times lower than in the radial-flow model after the same volume of gas injection. Similar behavior is shown for different volumes of gas injection (Fig. 15).
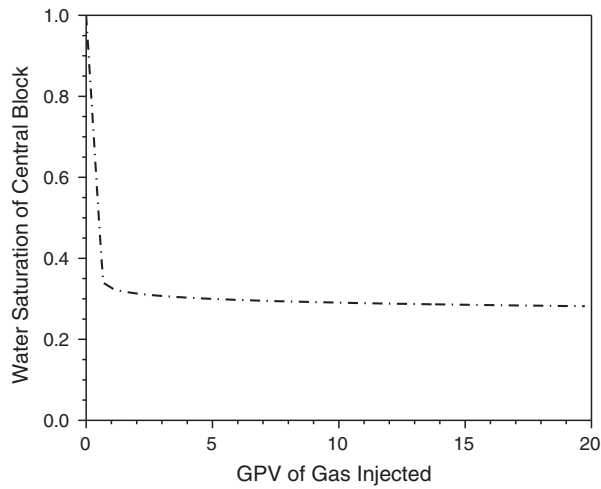
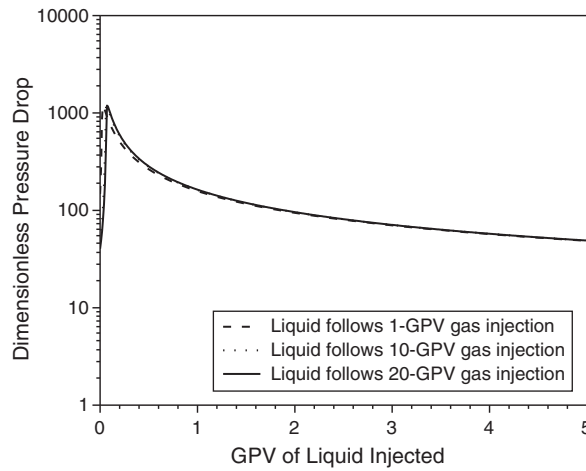**Fig. 12—Water saturation in the gridblock during gas injection.**

Fig. 13—Dimensionless pressure drop during liquid injection following various periods of gas injection, calculated with the Peaceman equation. The curves nearly overlie each other.
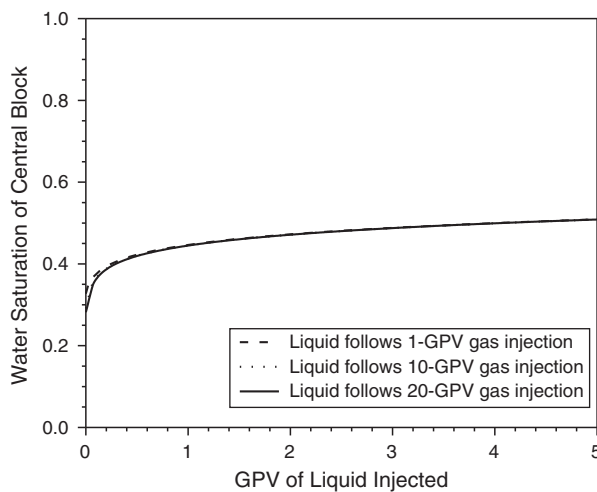
Fig. 14—Water saturation in the gridblock during liquid injection following various periods of gas injection. The curves nearly overlie each other.

Fig. 16 shows the comparison for liquid injectivity. On the basis of our experimental data in the radial-flow model, a larger gas slug injected before liquid injection increases the injectivity of the subsequent liquid slug. However, the effect of gas injection on the subsequent liquid injectivity is not represented by the conventional models based on the IT foam model and the Peaceman equation. The larger the gas slug injected before liquid, the greater the error in the simulation with the conventional model.
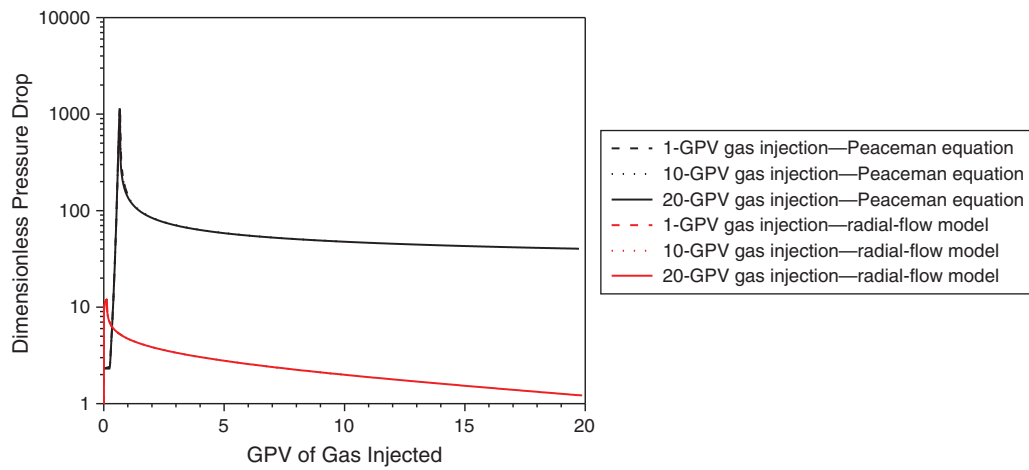
Fig. 15—Comparison of gas injectivity calculated with the Peaceman equation and with the radial-flow model. The dotted, dashed, and solid lines overlie each other in both (red and black) cases.
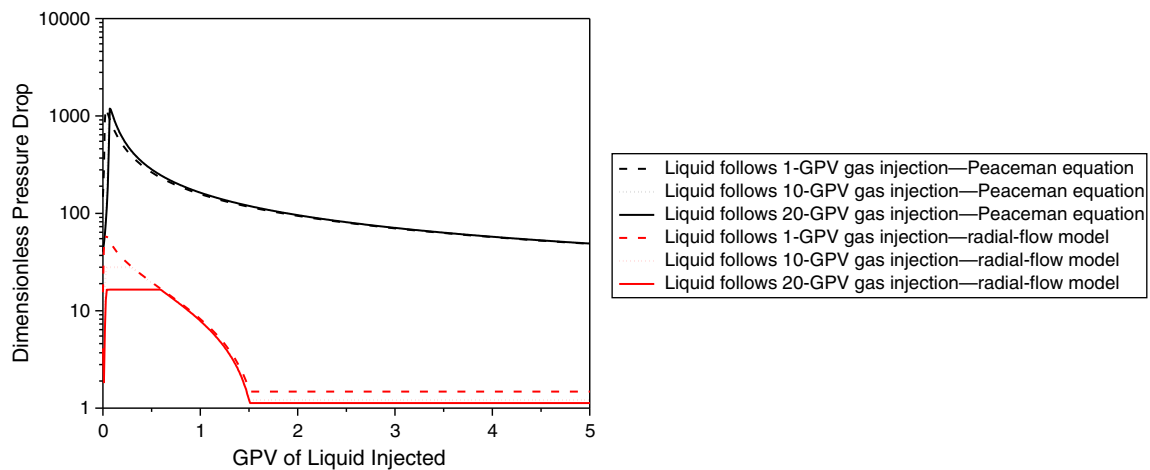
Fig. 16—Comparison of liquid injectivity calculated with Peaceman equation and with the radial-flow model. The dotted, dashed, and solid lines overlie each other in the Peaceman-equation case (black).

In **Figs. 17 and 18,** we seek to reconcile the results of the radial-flow model and the conventional model by applying a constant skin factor. For illustration, the skin factors for the gas- and liquid-injection periods are both assigned a value of $\left[\left(-\dfrac{24}{25}\right)\ln\dfrac{r_w}{r_e}\right]$. In other words, the rise in injection-well pressure is 1/25 of that predicted by the Peaceman equation without the skin factor.

Fig. 17—Dimensionless pressure drop during gas injection, calculated with the conventional Peaceman equation, the Peaceman equation with a constant skin factor, and the radial-flow model.

Fig. 18—Dimensionless pressure drop during liquid injection, calculated with the conventional Peaceman equation, the Peaceman equation with a constant skin factor, and the radial-flow model.

As shown in Fig. 17, the Peaceman equation with this skin factor underestimates gas injectivity by a factor of approximately 4 at the peak in P_D. After approximately 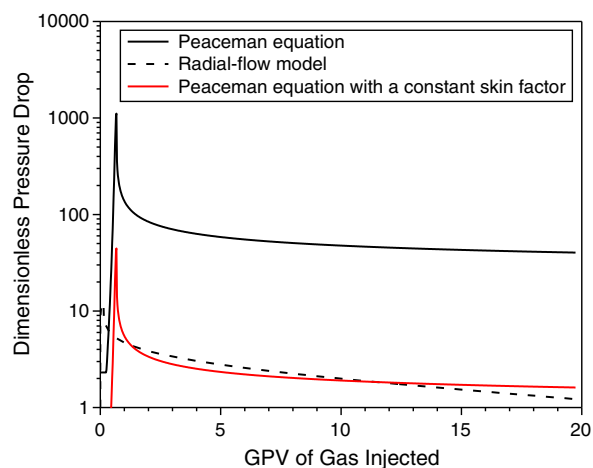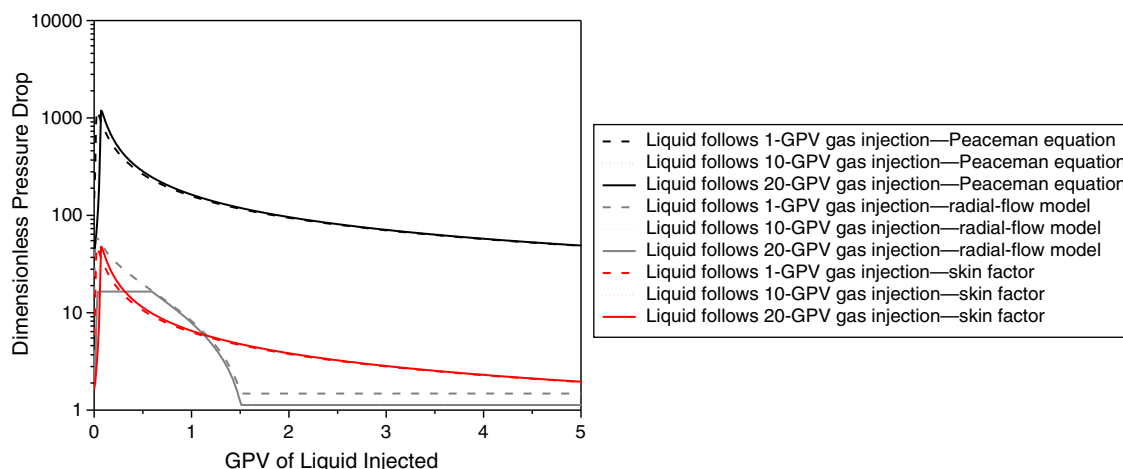1 GPV of gas injection, using the same skin factor either underestimates or overestimates gas injectivity by as much as 1.5. In general, the Peaceman equation with a constant negative skin factor can give a reasonably good approximation for gas injectivity.

Fig. 18 compares the solutions using the conventional Peaceman equation, the Peaceman equation with the same constant skin factor, and the radial-flow model for the liquid-injection period. The maximum error when using the constant skin factor is approximately a factor of 6 at 1.5-GPV liquid injection, when gas has fully dissolved into the injected liquid within the fingers in the region of interest. The errors at the short time depend on how much gas has been injected in the previous slug.

Discussion

As noted in the Introduction, poor liquid injectivity is a problem in SAG foam applications. In our modeling, liquid injectivity estimated from the radial-flow model is much better than that predicted by the simulator. Nonetheless, liquid injectivity can still be as much as 60 times worse than injectivity of water into a water-saturated formation (Fig. 16), and unintended fracturing during liquid injection is still a concern.

Limitations of the Study. The model we introduce is based directly on the laboratory data but contains many assumptions and approximations.

In coreflood experiments, the drying out and collapse of foam reflect the interplay of pressure gradients, capillary effects, and evaporation of liquid. The effects might not scale up easily to field scale, other pressure gradients, temperatures, or pressures. Representing the complete collapse of foam very near an injection well in many cases would require very fine grid refinement. In this study, the net result is that the conventional simulator underestimates the injectivity during liquid injection.

Gas within the trapped foam surrounding liquid fingers must expand as pressure falls during prolonged liquid injection. CT images in our previous study and in Nguyen et al. (2009b) show that gas saturation increases within this trapped gas region as pressure falls, but not enough to fully account for gas expansion. We do not know how this gas (and some liquid) escapes as pressure falls—that is, whether (slowly) through the trapped gas downstream or by way of the liquid finger. However, CT images, both in our previous study and in Nguyen et al. (2009b), clearly show that liquid saturation rises within the fingers at a rate roughly consistent with the expected rate of gas dissolution into unsaturated injected liquid.

In addition, fingering during liquid injection is difficult to extrapolate from the core scale to the radial flow around the injection well; it might also depend on the pressure gradient, which is a function of radial position and other factors. Fingering of liquid through trapped gas is important to liquid injectivity but difficult to represent in a simulator.

In the example examined here, a constant negative skin factor for gas and liquid injection brings the solutions of conventional models based on the Peaceman equation and the radial-flow model closer. Some deviations between the model and the data remain, and, thus, the radial-flow model is not quantitative when scaled up. However, it does give an idea of the deviations from simulations to be expected in field applications. A prudent operator should be prepared to adjust injection rates to take advantage of injectivity greater than expected from simulation or to prevent fracturing if injectivity is worse than expected.

Our experimental results, and therefore our modeling, depend on temperature, pressure, surfactant formulation, gas, porous medium, and other factors. In particular, the evaporation of water in the foam bank and dissolution of gas during liquid injection would depend on vapor pressure and solubilities of the gas and liquid. A new set of experiments and parameters fit to those results would be needed for each new field application.

Challenges for Foam Simulation. Foam simulation faces a variety of challenges. Accurate modeling of near-wellbore mobility changes requires very fine grid refinement, as discussed previously (see also Leeftink et al. 2015; Al Ayesh et al. 2017). Similar resolution is needed to represent shock fronts (Zanganeh et al. 2014). However, grid refinement will not be sufficient if the foam model itself does not adequately represent foam mobility.

During gas injection, the key is representing foam weakening and collapse as foam dries out. The simulator parameters are fit to the foam-quality-scan data in our study (Appendix A) and do not predict foam collapse as foam dries out. Even at irreducible water saturation (S_{wr}), the model predicts that foam reduces gas mobility by a factor of approximately 350. Rossen and Boeije (2015) show that a separate method is needed to fit parameters for gas injection in SAG, different from a least-squares fit to a conventional foam-quality scan. The Zanganeh et al. (2011) modification of the foam model can ensure foam collapse at S_{wr}; see also Al Ayesh et al. (2017). To our knowledge, however, this model is not used in any commercial simulator. Model fits with small values of *epdry* (Appendix A) are

especially problematic in this regard. In fitting the effect of long-time gas injection on foam mobility near a gas-injection well in a field test, Rossen et al. (2017) found that the Zanganeh model (Zanganeh et al. 2011) did a reasonable job of representing foam mobility after many PVs of gas injection. In any event, a model fit with more-abrupt foam collapse at the limiting water saturation would have come closer to the predictions of the radial-flow model during gas injection in this study.

During liquid injection, there are at least three challenges, in addition to grid refinement, to conventional foam simulation: representing liquid fingering through trapped gas, gas dissolution into liquid, and hysteresis in gas trapping. The last challenge might be the most severe for simulating liquid injectivity. The collapse of foam after a long period of gas injection in our study led to reduced gas trapping upon subsequent liquid injection, with a major effect on overall liquid injectivity. This effect is not represented in the conventional simulator model we used here. Without at least an approximate representation of these effects, grid refinement would not be sufficient to give an accurate simulation of liquid injectivity in a SAG foam process.

Conclusions

- In simulation of gas injectivity in a SAG process, conventional models based on the Peaceman equation, combined with the assumption of uniform saturation in the gridblock containing the injection well, can greatly underestimate the gas injectivity.
- The conventional models also underestimate the injectivity during liquid injection. They cannot represent the effect of previous gas injection on the subsequent liquid injectivity, especially the propagation of the collapsed-foam region, without very fine grid resolution near the well. Fundamentally, current foam models do not represent hysteresis in gas trapping between gas and liquid injection. Liquid fingering through foam and gas dissolution into liquid fingers are also part of the reason for the underestimation of injectivity.
- The process of coreflood experiments, model fitting, and extrapolation to radial flow described here could be applied in future field applications. In the case examined here, the conventional simulator based on the Peaceman equation works reasonably well with a constant skin factor for periods of gas injection and liquid injection.
- Our modeling indicates that real injectivity is better than that predicted by the conventional simulators in both gas and liquid injection. However, the radial-flow model, though based directly on laboratory data, includes many assumptions and simplifications. The operator should be prepared to adjust injection rates according to unexpected changes in injection pressure.
- The parameter values adopted in this study are based on our laboratory-scale experiments and might not be valid for other applications. For different field cases, one would need to conduct new experiments to recalculate the parameter values.

Nomenclature

A = cross-section area, m^2 (Eq. 3)
$epcap$ = parameter that controls non-Newtonian behavior in the low-quality regime, dimensionless
$epdry$ = parameter that controls the abruptness of the transition from low-quality-foam regime to high-quality regime, dimensionless
$fmcap$ = reference capillary number, dimensionless
$fmdry$ = water saturation at the transition from low-quality-foam regime to high-quality regime, dimensionless
$fmmob$ = reference gas-mobility-reduction factor, dimensionless
f_w = water fractional flow, dimensionless
FM = foam reduction factor, dimensionless (Eq. A-5)
F_1 = effect of surfactant concentration, dimensionless (Eq. A-5)
F_2 = effect of water saturation, dimensionless (Eqs. A-5 and A-6)
F_3 = effect of oil saturation, dimensionless (Eq. A-5)
F_4 = effect of gas velocity, dimensionless (Eq. A-5)
F_5 = effect of capillary number, dimensionless (Eq. A-5)
F_6 = effect of critical capillary number, dimensionless (Eq. A-5)
h = reservoir height, m
k = permeability, md
k_{rw} = water relative permeability, dimensionless
k_{rg} = gas relative permeability, dimensionless
k_{rg}^f = foam-reduced gas relative permeability, dimensionless
k_{rw}^o = endpoint water relative permeability, dimensionless
k_{rg}^o = endpoint gas relative permeability, dimensionless
l_1, l_2 = linear position, m (Eq. 3)
L = gridblock size, m
n_w, n_g = empirical parameter of Corey relative permeability definition, dimensionless
P_b = pressure in a gridblock in Peaceman-equation model, Pa (Eq. 10)
P_{r_e} = pressure at the outer radius for Peaceman-equation model, Pa (Eq. 10)
P_D = pressure difference in radial-flow model, dimensionless (Eq. 5)
P_W = pressure of an injection well for Peaceman-equation model, Pa (Eq. 11)
Q_g^{in} = volumetric gas-flow rate into a gridblock, m^3/s (Eq. 6)
Q_w^{in} = volumetric water-flow rate into a gridblock, m^3/s (Eq. 6)
Q_w^{out} = volumetric water-flow rate out a gridblock, m^3/s (Eq. 6)
Q_g^{out} = volumetric gas-flow rate out a gridblock, m^3/s (Eq. 6)
Q_t = total volumetric flow rate, m^3/s (Eq. 3)
r_1, r_2 = radial position, m (Eqs. 4, 5)
r_e = outer radius for Peaceman equation, m (Eq. 11)
r_w = wellbore radius, m (Eq. 11)
S_w = water saturation, dimensionless
S_{gr} = residual gas saturation, dimensionless
S_{wr} = irreducible water saturation, dimensionless
u_t = total superficial velocity, m/s
V = dimensionless velocity of bank propagation, dimensionless

ϕ = porosity, dimensionless
λ_w = water mobility, m²/Pa·s
λ_t = total mobility, m²/Pa·s
λ_{rt} = total relative mobility, dimensionless
Δp = pressure gradient, Pa/m
Δp_b = pressure difference across each bank for linear-flow and radial-flow models, Pa (Eqs. 3, 4)
Δp_F = pressure difference across the foam bank for linear-flow and radial-flow models, Pa (Eqs. 1, 2)
Δp_{FCG} = pressure difference across the collapsed-foam bank during gas injection for linear-flow and radial-flow models, Pa (Eq. 1)
Δp_{FCL} = pressure difference across the collapsed-foam bank during liquid injection for linear-flow and radial-flow models, Pa (Eq. 2)
Δp_{LF} = pressure difference across the liquid-fingering bank during liquid injection for linear-flow and radial-flow models, Pa (Eq. 2)
Δp_{GD} = pressure difference across the gas-dissolution bank during liquid injection for linear-flow and radial-flow models, Pa (Eq. 2)
Δp_t = total pressure difference for linear-flow and radial-flow models, Pa (Eq. 2)
ΔP_t = pressure difference between an injection well and the gridblock containing it, Pa (Eq. 11)
μ_w = water viscosity, Pa·s
μ_g = gas viscosity, Pa·s

Acknowledgments

References

Al Ayesh, A. H., Salazar, R., Farajzadeh, R. et al. 2017. Foam Diversion in Heterogeneous Reservoirs: Effect of Permeability and Injection Method. *SPE J.* **22** (5): 1402–1415. SPE-179650-PA. https://doi.org/10.2118/179650-PA.

Alvarez, J. M., Rivas, H. J., and Rossen, W. R. 2001. Unified Model for Steady-State Foam Behavior at High and Low Foam Qualities. Presented at SPE Annual Technical Conference and Exhibition, Houston, 3–6 October. SPE-56825-MS. https://doi.org/10.2118/56825-MS.

Boeije, C. S. and Rossen, W. R. 2015. Fitting Foam-Simulation-Model Parameters to Data: I. Coinjection of Gas and Liquid. *SPE Res Eval & Eng* **18** (2): 264–272. SPE-174544-PA. https://doi.org/10.2118/174544-PA.

Cheng, L., Reme, A. B., Shan, D. et al. 2000. Simulating Foam Processes at High and Low Foam Qualities. Paper presented at SPE/DOE Improved Oil Recovery Symposium, Tulsa, 3–5 April. SPE-59287-MS. https://doi.org/10.2118/59287-MS.

Computer Modeling Group Ltd. (CMG). 2006. STARS User's Guide. Calgary, Alberta, Canada: CMG.

Farajzadeh, R., Lotfollahi, M., Eftekhari, A. A. et al. 2015. Effect of Permeability on Implicit-Texture Foam Model Parameters and the Limiting Capillary Pressure. *Energy & Fuels* **29** (5): 3011–3018. https://doi.org/10.1021/acs.energyfuels.5b00248.

Gong, J., Vincent-Bonnieu, S., Kamarul Bahrim, R. Z. et al. 2018. Modelling of Liquid Injectivity in Surfactant-Alternating-Gas Foam Enhanced Oil Recovery. Presented at the SPE EOR Conference at Oil and Gas West Asia, Muscat, Oman, 26–28 March. SPE-190435-MS. https://doi.org/10.2118/190435-MS.

Gong, J., Vincent-Bonnieu, S., Kamarul Bahrim, R. Z. et al. 2019. Laboratory Investigation of Liquid Injectivity in Surfactant-Alternating-Gas Foam Enhanced Oil Recovery. *Transport in Porous Media* (in press; online 19 February 2019). https://doi.org/10.1007/s11242-018-01231-5.

Heller, J. P. 1994. CO₂ Foams in Enhanced Oil Recovery. In *Foams: Fundamentals and Applications in the Petroleum Industry*, ed. M. J. Comstock, Chap. 5, 201–234. *Advances in Chemistry*, Vol. 242. Washington, DC: American Chemical Society.

Kam, S. I., Nguyen, Q. P., Li, Q. et al. 2007. Dynamic Simulations With an Improved Model for Foam Generation. *SPE J.* **12** (1): 35–48. SPE-90938-PA. https://doi.org/10.2118/90938-PA.

Kapetas, L., Vincent Bonnieu, S., Farajzadeh, R. et al. 2017. Effect of Permeability on Foam-Model Parameters: An Integrated Approach From Core-flood Experiments Through to Foam Diversion Calculations. *Colloids and Surfaces A: Physicochemical and Engineering Aspects* **530** (Oct): 172–180. https://doi.org/10.1016/j.colsurfa.2017.06.060.

Khatib, Z. I., Hirasaki, G. J., and Falls, A. H. 1998. Effects of Capillary Pressure on Coalescence and Phase Mobilities in Foams Flowing Through Porous Media. *SPE Res Eval & Eng* **3** (3): 919–926. SPE-15442-PA. https://doi.org/10.2118/15442-PA.

Kibodeaux, K. R. and Rossen, W. R. 1997. Coreflood Study of Surfactant-Alternating-Gas Foam Processes: Implications for Field Design. Presented at the SPE Western Regional Meeting, Long Beach, California, 25–27 June. SPE-38318-MS. https://doi.org/10.2118/38318-MS.

Kibodeaux, K. R., Zeilinger, S. C., and Rossen, W. R. 1994. Sensitivity Study of Foam Diversion Processes for Matrix Acidization. Presented at the SPE Annual Technical Conference and Exhibition, New Orleans, 25–28 September, SPE-28550-MS. https://doi.org/10.2118/28550-MS.

Kovscek, A. R. and Radke, C. J. 1994. Fundamentals of Foam Transport in Porous Media. In *Foams: Fundamentals and Applications in the Petroleum Industry*, ed. M. J. Comstock, Chap. 3, 115–163. Advances in Chemistry, Vol. 242. Washington, DC: American Chemical Society.

Kuehne, D. L., Ehman, D. I., Emanuel, A. S. et al. 1990. Design and Evaluation of a Nitrogen-Foam Field Trial. *J Pet Technol* **42** (2): 504–512. SPE-17381-PA. https://doi.org.10.2118/17381-PA.

Lake, L. W., Johns, R. T., Rossen, W. R. et al. 2014. *Fundamentals of Enhanced Oil Recovery*. Richardson, Texas, USA: Society of Petroleum Engineers.

Leeftink, T. N., Latooij, C. A., and Rossen, W. R. 2015. Injectivity Errors in Simulation of Foam EOR. *J. Pet. Sci. Eng.* **126** (Feb): 26–34. https://doi.org/10.1016/j.petrol.2014.11.026.

Ma, K., Farajzadeh, R., Lopez-Salinas, J. L. et al. 2014. Non-Uniqueness, Numerical Artifacts, and Parameter Sensitivity in Simulating Steady-State and Transient Foam Flow Through Porous Media. *Transp Porous Med.* **102** (3): 325–348. https://doi.org/10.1007/s11242-014-0276-9.

Ma, K., Lopez-Salinas, J. L., Puerto, M. C. et al. 2013. Estimation of Parameters for the Simulation of Foam Flow Through Porous Media. Part 1: The Dry-Out Effect. *Energy & Fuels* **27** (5): 2363–2375. https://doi.org/10.1021/ef302036s.

Martinsen, H. A. and Vassenden, F. 1999. Foam-Assisted Water Alternating Gas (FAWAG) Process on Snorre. Presented at the 10th European IOR Symposium, Brighton, UK, 18–20 August. https://doi.org/10.3997/2214-4609.201-406335.

Matthews, C. S. 1989. Carbon Dioxide Flooding. In *Developments in Petroleum Science*, eds. E. C. Donaldson, G. V. Chilingarian, and T. F. Yen, Chap. 6, 129–156. Amsterdam, The Netherlands: Elsevier.

Nguyen, Q. P., Currie, P. K., and Zitha, P. L. J. 2003. Determination of Foam Induced Fluid Partitioning in Porous Media Using X-Ray Computed Tomography. Presented at the International Symposium on Oilfield Chemistry, Houston, 5–7 February. SPE-80245-MS. https://doi.org/10.2118/80245-MS.

Nguyen, Q. P., Rossen, W. R., Zitha, P. L. J. et al. 2009a. Determination of Gas Trapping With Foam Using X-Ray Computed Tomography and Effluent Analysis. *SPE J.* **14** (2): 222–236. SPE-94764-PA. https://doi.org/10.2118/94764-PA.

Nguyen, Q. P., Zitha, P. L. J., Currie, P. K. et al. 2009b. CT Study of Liquid Diversion With Foam. *SPE Prod. & Oper.* **24** (1): 12–21. SPE-93949-PA. https://doi.org/10.2118/93949-PA.

Patzek, T. W. and Myhill, N. A. 1989. Simulation of the Bishop Steam Foam Pilot. Presented at the SPE California Regional Meeting, Bakersfield, California, 5–7 April. SPE-18786-MS. https://doi.org/10.2118/18786-MS.

Peaceman, D. W. 1978. Interpretation of Well-Block Pressures in Numerical Reservoir Simulation. *SPE J*. **18** (3): 183–194. SPE-6893-PA. https://doi.org/10.2118/6893-PA.

Rossen, W. R. 1996. Foams in Enhanced Oil Recovery. In *Foams: Theory, Measurements and Applications*, eds. R. K. Prud'homme and S. Khan, Chap. 11, 413–464. New York: Marcel Dekker.

Rossen, W. R. 2013. Numerical Challenges in Foam Simulation: A Review. Presented at the SPE Annual Technical Conference and Exhibition, New Orleans, 30 September–2 October. SPE-166232-MS. https://doi.org/10.2118/166232-MS.

Rossen, W. R. and Boeije, C. S. 2015. Fitting Foam-Simulation-Model Parameters to Data: II. Surfactant-Alternating-Gas Foam Applications. *SPE Res Eval & Eng* **18** (2): 273–283. SPE-165282-PA. https://doi.org/10.2118/165282-PA.

Rossen, W. R., Ocampo-Florez, A. A., Restrepo, A. et al. 2017. Long-Time Diversion in SAG Foam Enhanced Oil Recovery From a Field Test. *SPE Res Eval & Eng* **20** (1): 1–7. SPE-170809-PA. https://doi.org/10.2118/170809-PA.

Rossen, W. R., van Duijn, C. J., Nguyen, Q. P. et al. 2010. Injection Strategies to Overcome Gravity Segregation in Simultaneous Gas and Water Injection Into Homogeneous Reservoirs. *SPE J*. **15** (1): 76–90. SPE-99794-PA. https://doi.org/10.2118/99794-PA.

Schlumberger. 2010. ECLIPSE Industry-Reference Reservoir Simulator. Houston, Texas: Schlumberger.

Schramm, L. L. 1994. *Foams: Fundamentals and Applications in the Petroleum Industry*. Washington, DC: *Advances in Chemistry*, Vol. 242, Washington, DC: American Chemical Society.

Shan, D. and Rossen, W. R. 2004. Optimal Injection Strategies for Foam IOR. *SPE J*. **9** (2): 132–150. SPE-88811-PA. https://doi.org/10.2118/88811-PA.

STARS™ is a trademark of Computer Modelling Group Ltd., 3710 33 Street NW, Calgary, Alberta, T2L 2M1, Canada.

Zanganeh, M. N., Kam, S. I., LaForce, T. et al. 2011. The Method of Characteristics Applied to Oil Displacement by Foam. *SPE J*. **16** (1): 8–23. SPE-121580-PA. https://doi.org/10.2118/121580-PA.

Zanganeh, M. N., Kraaijevanger, J. F. B. M., Buurman H. W. et al. 2014. Challenges to Adjoint-Based Optimization of a Foam EOR Process. *Computat. Geosci*. **18** (3–4): 563–577. https://doi.org/10.1007/s10596-014-9412-4.

Zeilinger, S. C., Wang, M., Kibodeaux, K. R. et al. 1995. Improved Prediction of Foam Diversion in Matrix Acidization. Presented at the SPE Production Operations Symposium, Oklahoma City, Oklahoma, 2–4 April. SPE-29529-MS. https://doi.org/10.2118/29529-MS.

Zhou, Z. and Rossen, W. R. 1995. Applying Fractional-Flow Theory to Foam Processes at the "Limiting Capillary Pressure". *SPE Advanced Technology Series* **3** (1): 154–162. SPE-24180-PA. https://doi.org/10.2118/24180-PA.

Appendix A

Here, we briefly introduce the IT model in the STARS™ simulator (Cheng et al. 2000; CMG 2006), and the approaches for fitting foam-model parameters.

In the absence of foam, the water and gas relative permeabilities are defined as

$$k_{rw} = k_{rw}^o S^{n_w}, \dots\dots\dots\dots\dots\dots\dots\dots\dots\dots\dots\dots\dots\dots\dots\dots\dots\dots\dots\dots \text{(A-1)}$$

$$k_{rg} = k_{rg}^o (1 - S)^{n_g}, \dots\dots\dots\dots\dots\dots\dots\dots\dots\dots\dots\dots\dots\dots\dots\dots\dots\dots\dots \text{(A-2)}$$

$$S \equiv \frac{S_w - S_{wr}}{1 - S_{wr} - S_{gr}}, \dots\dots\dots\dots\dots\dots\dots\dots\dots\dots\dots\dots\dots\dots\dots\dots\dots\dots\dots \text{(A-3)}$$

where S_w, S_{wr}, and S_{gr} are the water saturation, the irreducible water saturation, and the residual gas saturation, respectively; n_w and n_g are empirical parameters; and k_{rw}^o and k_{rg}^o are the endpoint water and gas relative permeabilities, respectively. We use the parameter values reported by Kapetas et al. (2017) for Berea sandstone The value of S_{wr} is adapted according to our CT-scan experiments. The values are listed in **Table A-1**. Water and gas viscosities are 3.2×10^{-4} Pa·s and 2.0×10^{-5} Pa·s, respectively.

Parameter	Units	Value
n_g	–	1.22
n_w	–	5.25
k_{rg}^o	–	0.47
k_{rw}^o	–	0.14
S_{gr}	–	0.25
S_{wr}	–	0.204

Table A-1—Corey relative permeability parameters.

In this study, we use an IT foam model that is widely used in the simulator STARS (Cheng et al. 2000, CMG 2006). The gas mobility is reduced from the foam-free value k_{rg} to k_{rg}^f by a foam-reduction factor *FM*:

$$k_{rg}^f = k_{rg} \cdot FM. \dots\dots\dots\dots\dots\dots\dots\dots\dots\dots\dots\dots\dots\dots\dots\dots\dots\dots\dots\dots \text{(A-4)}$$

FM is defined as follows:

$$FM = \frac{1}{1 + fmmob \cdot F_1 \cdot F_2 \cdot F_3 \cdot F_4 \cdot F_5 \cdot F_6}, \dots\dots\dots\dots\dots\dots\dots\dots\dots\dots\dots\dots\dots \text{(A-5)}$$

where the parameter *fmmob* is the reference gas-mobility-reduction factor for wet foams. This parameter corresponds to the maximum-attainable mobility reduction. The functions represent the following different physical effects: surfactant concentration (F_1), water saturation (F_2), oil saturation (F_3), gas velocity (F_4), capillary number (F_5), and the critical capillary number (F_6). In fitting a SAG injection process in this study, only function F_2 is taken into account. The function F_2 is given by

$$F_2 = 0.5 + \frac{\arctan[epdry \cdot (S_w - fmdry)]}{\pi}, \quad \dots\dots\dots\dots\dots\dots\dots\dots\dots\dots\dots\dots\dots\dots\dots\dots\dots\dots\dots (A\text{-}6)$$

where *epdry* is the parameter that controls the abruptness of the transition from the low-quality regime to the high-quality regime, and *fmdry* is the water saturation at the transition. Function F_2 controls the high-quality regime, which is crucial to injectivity in a SAG process (Rossen and Boeije 2015).

Different approaches for fitting foam-model parameters have been proposed in literature (Cheng et al. 2000; Ma et al. 2013, 2014; Boeije and Rossen 2015; Rossen and Boeije 2015). Boeije and Rossen (2015) proposed a method for fitting foam parameters to pressure-gradient data as a function of foam quality (gas fractional flow) at a single superficial velocity (i.e., a "foam-quality scan"). In this study, we adopt the method of Boeije and Rossen (2015) to obtain a first estimate of the foam parameters by fitting a foam-quality scan for the same surfactant formulation and coreflood conditions as in the other experiments described here. We then use the least-squares optimization routine of Farajzadeh et al. (2015) to refine the fit; the result is shown in **Fig. A-1.** Because the data include the low-quality-foam regime in both cases, which is strongly affected by shear thinning (Cheng et al. 2000, Alvarez et al. 2001, Boeije and Rossen 2015), we included the function F_5 in the fit to the foam-scan data. Otherwise, the fit of parameters crucial to the high-quality regime (*epdry* in particular) can be distorted. We do not use function F_5 in the SAG foam simulations, however, because injectivity during gas injection is dominated by the high-quality regime (Rossen and Boeije 2015). The values of foam parameters are listed in **Table A-2.** Although we fit the parameters *epcap* and *fmcap* to the foam scan, we leave them out for the modeling of injectivity in this paper, because as noted, they mainly affect the low-quality regime. [In Table A-2 we have corrected an error in the earlier version of this paper. (Gong et al. 2018) regarding the adjustment of the value of *fmmob* after excluding the effects of parameters *epcap* and *fmcap*. This change makes no substantial difference to our conclusions.]
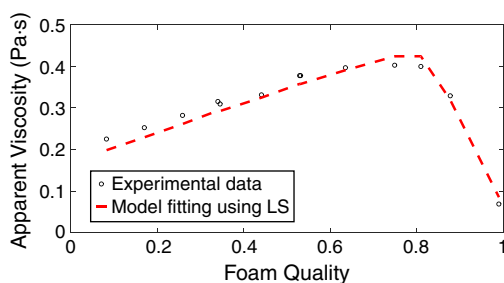

Fig. A-1—Fitting foam parameters to single scan of apparent viscosity vs. foam quality (gas fractional flow).

Parameter	Units	Value
fmdry	–	0.35
epdry	–	3.2×10^2
fmmob	–	5.1×10^4
epcap	–	0.8
fmcap	–	2.0×10^{-7}

Table A-2—Foam parameters extracted from Figure A-1.

Jiakun Gong is a post-doctoral-degree researcher at Delft University of Technology, The Netherlands. He holds a PhD degree from Delft University of Technology. Gong's current research interests include flow in naturally fractured reservoirs, foam EOR, and gas trapping.

Sebastien Vincent-Bonnieu is a reservoir engineer at Shell Global Solutions International. He is also a researcher at Delft University of Technology. Vincent-Bonnieu's current research interests include gas/chemical EOR and carbon capture usage and storage.

Ridhwan Zhafri Kamarul Bahrim is a petroleum engineer specializing in reservoir engineering. He has worked for the research-and-development division of the Malaysian National Oil Company, Petronas, since 2010. Kamarul Bahrim has been involved as a reservoir technologist in various projects, which cover the aspects of production enhancement, EOR, field development planning, and EOR pilot implementations in Peninsular and East Malaysia. He also works with Shell through joint research and development to find the best solutions for field rejuvenation and facility improvement. Kamarul Bahrim graduated from the Colorado School of Mines with a degree in petroleum engineering in 2009. He has been a member of SPE since 2010.

Che Abdul Nasser Bakri Che Mamat is currently working as staff reservoir technologist at Petronas. He has 17 years' experience in the oil and gas industry with various projects and companies. Che Mamat has in-depth technical knowledge and capabilities in evaluating petroleum fluid analysis and chemical (foam, polymer, and surfactant) and thermal (light-oil air injection) EOR processes for Petronas's local and international assets. He was involved in the planning and execution of a well-intervention program using coiled tubing before joining Petronas. Che Mamat is also an active trainer in his area of expertise, to develop Petronas employees. His main interests include laboratory analysis, reservoir simulation, and pilot implementation of EOR processes.

Raj Deo Tewari is currently working as Custodian and Group Technical Authority in reservoir engineering at Petronas. He has 34 years' experience in the oil and gas industry as a practicing reservoir engineer and researcher. Tewari is involved with EOR research in Petronas. He is an industry adviser at the University Technology Petronas and chair of technology research in Petronas. Tewari's main interests include field development planning, reservoir management and surveillance, and EOR. He received the 2015 SPE Asia Pacific Technical Award.

Jeroen Groenenboom is currently the manager of chemical EOR technology for Shell at its Amsterdam Technology Centre. He has worked in various locations for Shell (The Netherlands, Russia, Qatar, Malaysia, China) in various roles in upstream development since 2001. Groenenboom's educational background is in geophysics (MSc degree from Utrecht University), and he holds a PhD degree (cum laude) from Delft University in hydraulic-fracture monitoring.

Rouhi Farajzadeh currently works as a reservoir engineer for Shell. He is also a part-time assistant professor at Delft University of Technology and an adjunct professor at Rice University. He holds MS (cum laude) and PhD (cum laude) degrees in reservoir engineering, both from Delft University of Technology, and a BS degree in chemical engineering from Tehran Polytechnic. Farajzadeh is an executive editor for the Journal of Petroleum Science and Engineering and serves as a technical editor for SPE peer-reviewed journals. He is the recipient of the 2018 SPE North Sea Regional Reservoir Description and Dynamics Award.

William Rossen is professor of reservoir engineering in the Department of Geoscience and Engineering at Delft University of Technology. His current research concerns use of foams for diverting fluid flow in porous media, modeling complex transport processes in networks, and understanding flow in naturally fractured geological formations. In 2011, Rossen was named Best Instructor at Delft University of Technology. In 2012, he was named an IOR Pioneer at the SPE/DOE Symposium on Improved Oil Recovery, Tulsa. Rossen is an SPE Distinguished Member.